# Temperature influence on the crystal structure of CdTe (111) films grown by molecular-beam epitaxy on GaAs (100) substrates

© E.A. Klimov<sup>1</sup>, A.N. Vinichenko<sup>1,2</sup>, I.S. Vasil'evskii<sup>1,2</sup>, A.N. Klochkov<sup>1,2</sup>, S.S. Pushkarev<sup>3</sup>, I.D. Burlakov<sup>1</sup>

117105 Moscow, Russia

E-mail: klimov\_evgenyi@mail.ru

Received March 6, 2025 Revised June 5, 2025 Accepted June 19, 2025

In this paper, we present the results of CdTe film growth by molecular beam epitaxy at different temperatures on undoped semi-insulating GaAs substrates with the crystallographic surface orientation (100) without a seed layer. Preparation of an atomically clean substrate surface with subsequent synthesis of GaAs and CdTe films were carried out in a single ultrahigh vacuum system with in-situ control by reflection high-energy electron diffraction and pyrometry. Using high-resolution X-ray diffractometry, photoluminescence spectroscopy and atomic force microscopy, the effect of growth temperature on the structural quality of epitaxial CdTe films was studied. It was shown that the synthesized epitaxial CdTe films have a predominant crystallographic orientation (111) with twinning, and their crystalline quality monotonically improves with an increase in the substrate growth temperature to 450 °C.

Keywords: molecular beam epitaxy, CdTe, cadmium telluride, twinning defects, single crystal.

DOI: 10.61011/SC.2025.03.61557.7673

# 1. Introduction

To date, molecular beam epitaxy (MBE) is one of the key technologies for the growth of HgCdTe structures both on matched (isotypic) substrates Cd<sub>0.96</sub>Zn<sub>0.04</sub>Te [1-3] and on mismatched substrates crystal lattice on (alternative) substrates, the advantage of which is lower cost and a larger area. Recently, more attention has been paid to the growth of high-quality single-crystal CdTe and CdZnTe transition buffer layers on alternative substrates (gallium arsenide [4,5], gallium antimonide [6,7], silicon [8,9] and germanium [10]) by the MBE method, with the subsequent growth of heteroepitaxial structures based on a triple solid solution of mercury-cadmium-telluride (HgCdTe), which occupy a leading position in the global market among materials for the manufacture of IR photodetectors [11–13] and function, depending on the composition, in all major windows of transparency of the Earth's atmosphere [14,15]. Optimization of growth technology is developing both in the direction of searching for more advantageous surface orientations of GaAs and Si monocrystalline substrates, and in the direction of searching for growth techniques for the formation of germ and buffer layers. In order to fully realize the advantages of alternative substrates for producing inexpensive and highly efficient photodetectors, it is necessary not only to master the process of epitaxial growth of active HgCdTe layers, but also to develop a technology for producing high-quality transient buffer layers that will be able to provide a low density of defects

in the active region of the heterostructure. The most important thing is to reduce the density of germinating dislocations and maintain a high degree of crystallinity of the material, these factors are influenced by the formation of transitional nanolayers between the substrate and the active region of the heterostructure. The main problem of the growth of highly perfect CdTe layers on GaAs or Si substrates is a significant mismatch of the lattice parameters:  $\sim 14\%$  between CdTe and GaAs [16] and  $\sim 19\,\%$  between CdTe and Si [17]. The researchers also tested growth on "high-index" GaAs(301) and Si(301) substrates, while observing a different density gradient of germinating dislocations in thick  $(7 \mu m)$  CdTe layers grown on such substrates [17]. However, manufacturing substrates of industrially compatible diameters with a high-index orientation is quite a costly task compared to substrates of conventional orientations (100) and (111).

The production of CdTe layers on GaAs(100) substrates of both orientations (100) and (111) is described in the literature, depending on a number of factors, including the surface condition: it was found in Ref. [18] that chemical treatment and features of high-temperature desorption of surface oxides affect for the nucleation of CdTe phases with orientation (100) or (111). Postgrowth annealing [19] or the introduction of ZnTe/CdTe superlattices [20] improves the crystal structure of CdTe(100). It was noted that the surface of CdTe(111) has a smoother morphology than CdTe(100), which may be related to the distribution of elastic deforma-

<sup>&</sup>lt;sup>1</sup> Orion R & P Association, JSC,

<sup>111538</sup> Moscow, Russia

<sup>&</sup>lt;sup>2</sup> National Research Nuclear University "MEPhl",

<sup>115409</sup> Moscow, Russia

<sup>&</sup>lt;sup>3</sup> National Research Center "Kurchatov Institute",

| <u>№</u><br>sample | $T_g$ , °C | Surface morphology of   | $S_q$ , nm              |                              |                           |
|--------------------|------------|---|-------------------------|------------------------------|---------------------------|
|                    |            |   | $5\times5\mu\mathrm{m}$ | $10 \times 10 \mu\mathrm{m}$ | $30\times30\mu\mathrm{m}$ |
| 8                  | 250        | Isotropic relief; rounded islands with size $0.1-0.2\mu\text{m}$ and up to $100\text{nm}$   | 17.4                    | 17.0                         | 15.2                      |
| 9                  | 325        | Isotropic relief; fine grains of irregular shape with size $0.04-0.06\mu\mathrm{m}$   | 5.4                     | 4.9                          | 3.5                       |
| 18                 | 400        | Isotropic relief; rounded flat islands with size $0.4-0.6\mu\text{m}$ and up to $4\text{nm}$ high   | 0.83                    | 0.85                         | 0.94                      |
| 15                 | 450        | Faceted relief with triangular steps with size $1-3\mu{\rm m}$ and angles $60^\circ;$ meander-shaped depressions with element lengths of $4-10\mu{\rm m}$ | 0.73                    | 1.17                         | 1.54                      |

Table 1. Surface morphology of grown CdTe films and their root-mean-square roughness

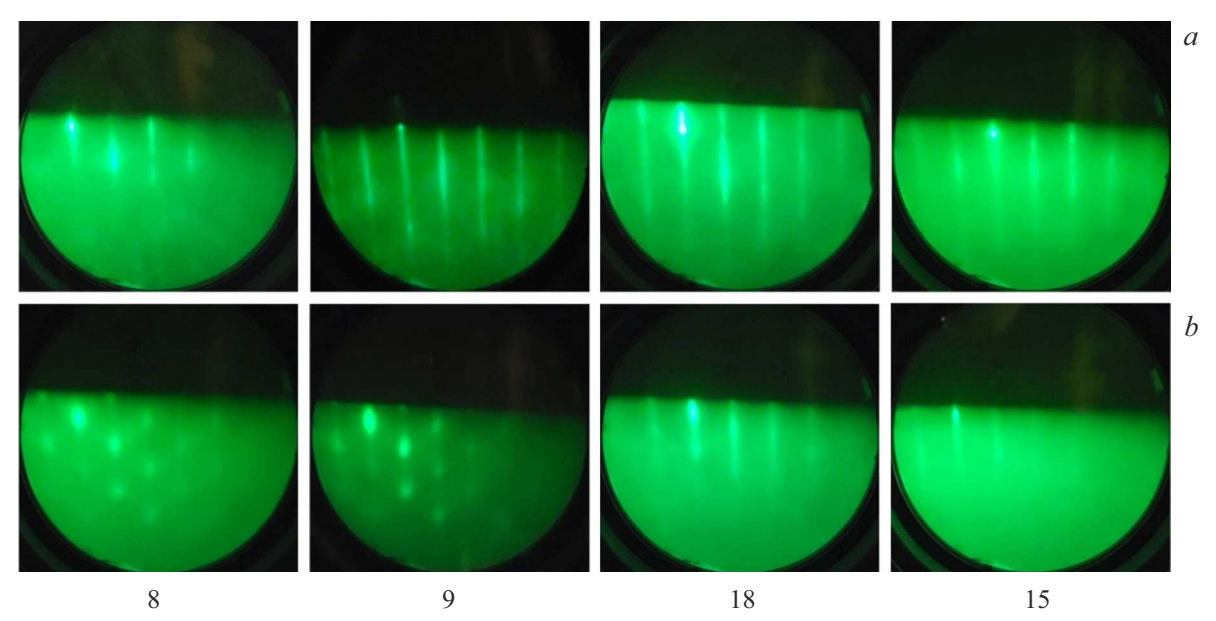


**Figure 1.** The RHEED pattern of samples 8, 9, 18, and 15 before the beginning (a) and at the fifth minute (b) of CdTe film growth on GaAs(100).

tions [20]. One of the well-known techniques for stabilizing the CdTe(100) phase when growing at GaAs(100) is the use of an intermediate ZnTe sublayer before CdTe growth, since the mismatch of the ZnTe crystal lattice parameter ( $a=6.1037\,\text{Å}$ ) relative to GaAs ( $a=5.6533\,\text{Å}$ ) is significantly lower than for CdTe ( $a=6.481\,\text{Å}$ ) [21]. In this work, on the contrary, the features of CdTe growth were studied without using a ZnTe sublayer: for example, when there is no effusion source of zinc or ZnTe in the installation, but an epitaxial CdTe layer with low surface roughness is required.

Thus, the relevance of conducting research to improve the structural properties of CdTe layers on GaAs substrates may be motivated by the possibility of synthesizing photosensitive heteroepitaxial structures of instrument quality on relatively inexpensive substrates, which should undoubtedly lead not only to an increase in the size of the photodetector matrix, but also to a reduction in their cost compared to more expensive and smaller ones. substrates Cd<sub>0.96</sub>Zn<sub>0.04</sub>Te.

The purpose of this paper is to comprehensively study the effect of growth temperature on the structural properties of CdTe films grown directly on the surface of GaAs(100) without the use of additional transition layers.

## 2. Samples and research methods

CdTe films were synthesized by molar beam epitaxy (MBE) on a robotic ultrahigh vacuum multi-chamber Riber Epineat Cluster on semi-insulating epi-ready GaAs substrates with crystallographic surface orientation (001) without a ZnTe germ buffer layer at various substrate temperatures. Temperature was controlled using a thermocouple integrated into the sample heater and *in situ* by pyrometric method using calibrated Ircon Modline 3

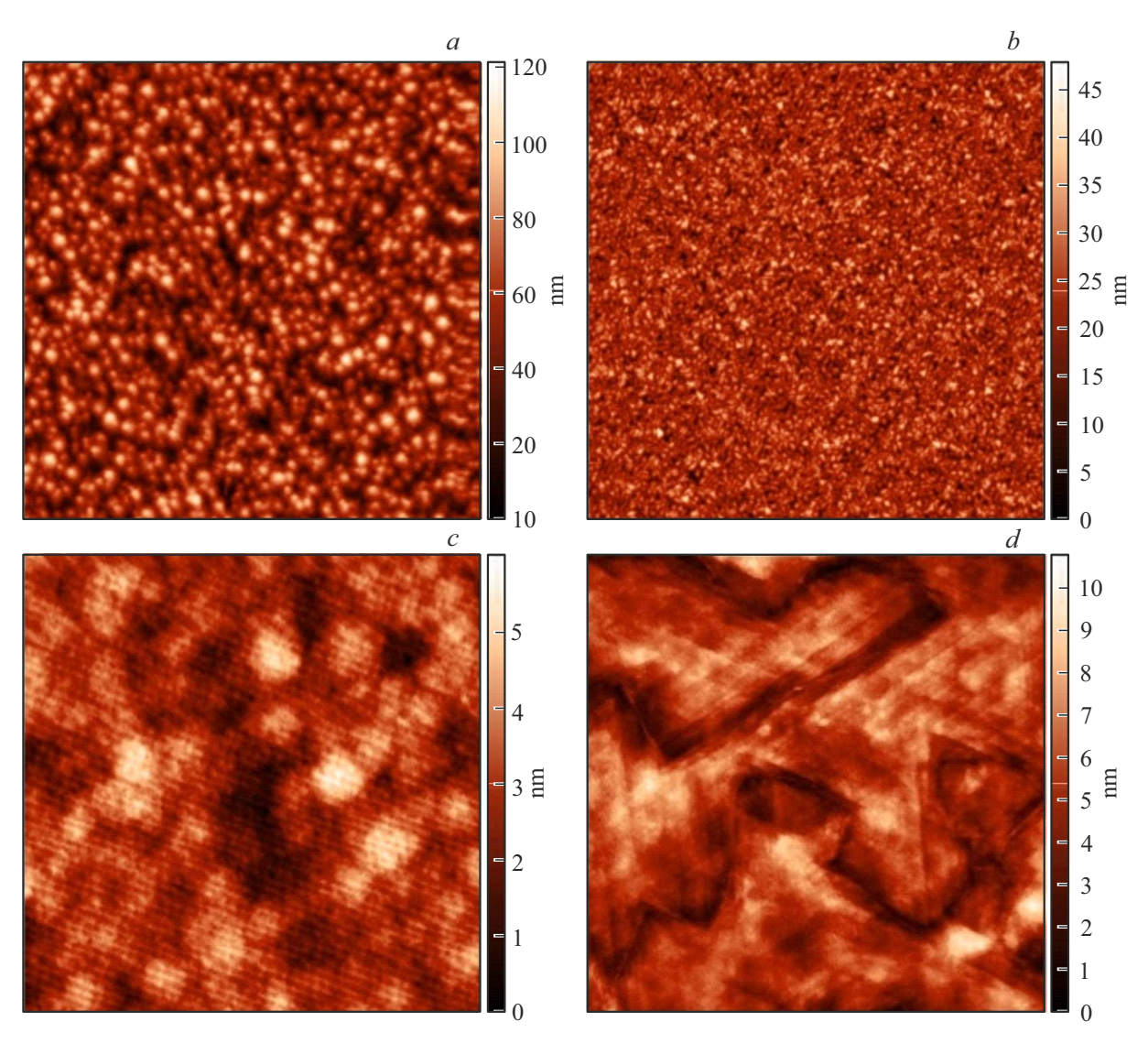


**Figure 2.** AFM images of the surface of grown films: a — sample 8,  $5 \times 5 \mu \text{m}$ ; b — sample 9,  $5 \times 5 \mu \text{m}$ ; c — sample 18,  $5 \times 5 \mu \text{m}$ ; d — sample 15,  $30 \times 30 \mu \text{m}$ .

pyrometers in the growth chamber of elements of group A<sup>III</sup>B<sup>V</sup> and Ircon Modline 5 in the growth chamber of elements of Group AIIBVI. The growth of the films was controlled in situ using a reflected high-energy electron diffraction (RHEED) system. A retractable Bayard-Alpert sensor was used to measure molecular flows. The pregrowth preparation of the GaAs substrate was carried out in several stages. The pre-degassing of the sample holder with a substrate from volatile compounds and water vapor was carried out in a separate pre-treatment chamber at a temperature of 300 °C for 20 minutes. After that, the holder with the substrate was placed in the growth chamber A<sup>III</sup>B<sup>V</sup>, where oxides were distilled from the substrate surface at a temperature of 640 °C in an arsenic stream. After that, the substrate temperature was reduced to 590 °C and an undoped GaAs buffer layer with a thickness of 500 nm was grown. Upon completion of the growth of the GaAs buffer

layer in growth chamber AIIIBV, the surface underwent an arsenic-stabilized reconstruction  $(2\times4)$ . The arsenic flow was blocked after cooling the plate to a temperature of  $\sim 200\,^{\circ}\text{C}$ . Next, the holder with the substrate was moved through vacuum to the growth chamber AIIBVI, in which CdTe films were grown at various growth temperatures. The Cd and Te streams generated by a single CdTe sublimation source were the same for all samples. The samples differed in substrate temperature during the growth of CdTe layers, as shown in Table 1. The sample 18 is characterized by a 2-fold increase in growth time (and hence thickness) relative to the rest of the samples. The growth rate was  $2\mu$ m/h. Figure 1 shows the reflection diffraction patterns of fast electrons obtained before and after the fifth minute of CdTe film growth on a GaAs(100) substrate. RHEED patterns were analyzed to assess the condition of the surface; surface reconstruction during growth in chamber A<sup>II</sup>B<sup>VI</sup> was not studied. A distinct pattern in the form of strands characteristic of a 2D smooth surface was observed at the initial stage, when the substrate was heated to the growth temperature. The dynamics of the RHEED patterns during the formation of CdTe films differed. Figure 1, *b* shows the RHEED patterns at the 5th minute of the growth of CdTe layers. For samples 8 and 9 grown at lower substrate temperatures, a three-dimensional growth regime was formed, as can be seen from the predominantly point reflexes of the RHEED, while the clarity of the reflexes was worse in sample 8. For samples 18 and 15 grown at a higher surface temperature, the growth regime corresponded to a two-dimensional one, which was observed by maintaining sufficiently clear extended strands in the RHEED paintings.

The morphology of the surface of the samples was studied by atomic force microscopy (AFM) on an NT-MDT Ntegra Maximus microscope in semi-contact mode, areas of  $5\times 5$ ,  $10\times 10$  and  $30\times 30\,\mu m$  were scanned.

Photoluminescence (PL) spectra were measured in an optical cryostat at a temperature of 77 K. To excite PL, radiation from a solid-state laser with a wavelength of 532 nm was used, focused on the sample surface into a spot with a size of  $\sim 150\,\mu m$  and a power density of  $\sim 1900\,W/cm^2.$  The PL signal in the range 1.2–2.0 eV was detected by a photoelectron multiplier FEU-62 cooled with liquid nitrogen.

High-resolution X-ray diffraction in a two-crystal scheme was used to evaluate the crystal structure of CdTe films. X-ray radiation from  $\text{Cu}K_{\alpha 1}$  copper ( $\lambda = 1.5406\,\text{Å}$ ) was used, which was monochromatized and collimated by a crystal  $\text{Ge}(220) \times 2$ .

## 3. Results and discussion

Figure 2 shows AFM images of the surface of grown CdTe films. The scale of the last image (Figure 2, d) was chosen to be smaller than the previous three (Figure 2, a-c) in order to capture the major features of the morphology of the sample surface 15. The values of the RMS roughness  $S_q$  of the surface of the grown CdTe layers are presented in Table 1. It can be seen that the surface roughness reaches a minimum at a growth temperature of  $400\,^{\circ}$ C. In comparison with the more uniform surface roughness of CdTe films grown at  $250-400\,^{\circ}$ C, we note the heterogeneous surface morphology of CdTe films grown at  $450\,^{\circ}$ C: meander-shaped dips and smooth the areas between them are covered with triangular 60-degree steps. In this regard, as the AFM scanning area increases, the RMS roughness value for sample 15 increases significantly, unlike other samples.

Figure 3 shows the X-ray diffraction reflection curves measured in the geometry  $2\theta/\omega$ . The scattering vector is oriented normal to the sample surface parallel to the reflection (004) of the GaAs substrate. Several peaks corresponding to the GaAs substrate and CdTe layers were detected on the RC in the angle range of  $20-80^{\circ}$ . Reflections (111), (222), and (333) CdTe are observed on

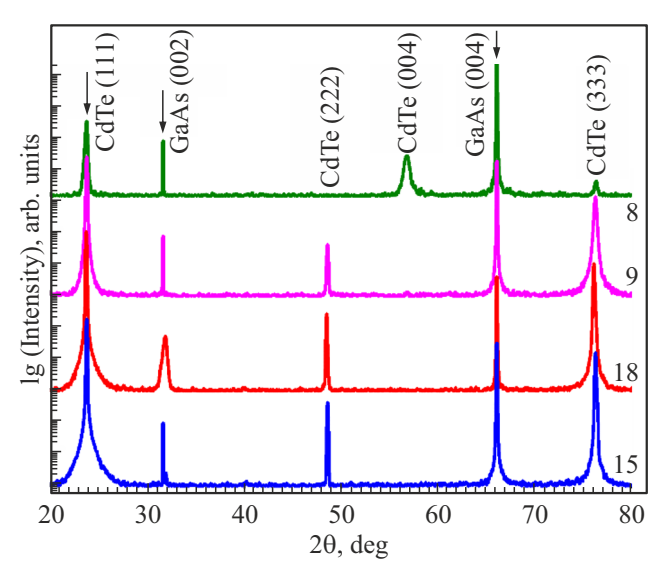


**Figure 3.** Overview RC in  $2\theta/\omega$ -geometries with the scattering vector oriented parallel to the direction (001) of the GaAs substrate (graphs are vertically offset for ease of comparison).

the RC of samples 9, 15, and 18, corresponding to several diffraction orders from CdTe layers with crystallographic orientation (111). Sample 8 stands out: for it, the CdTe(111) and (333) peaks are less intense than the peaks from the GaAs substrate, and the CdTe(222) peak is not observed, instead there is a peak at  $2\theta = 56.77^{\circ}$ , corresponding to the reflection of CdTe(004). Thus, CdTe films obtained at an epitaxial growth temperature of  $T_g \ge 325$  °C have a predominant crystallographic orientation (111). Lowering the growth temperature to  $T_g = 250\,^{\circ}\mathrm{C}$  leads to the formation of a polycrystalline film containing grains of various orientations. The polycrystalline CdTe structure for sample 8 was also confirmed by measuring the angular dependence of X-ray reflection on angle  $2\theta$  at a fixed grazing angle of incidence, at which reflections from CdTe grains of various orientations were also detected (figure not shown).

The intensity and half-width of the main peak of CdTe(111) differ for all samples, which shows differences in the crystal structure. Figure 4, a shows in more detail the shape of the RC of CdTe(111) measured in the mode of  $2\theta/\omega$  scanning, and Figure 4, b shows the corresponding rocking curves of the peak of CdTe(111); the half-widths of these peaks are provided in Table 2. The RC, Figure 4, a shows a mismatch between the position of the experimental peaks of CdTe(111) and the value calculated using the Wolfe-Bragg formula for samples 8, 9, and 18. This indicates a stretching deformation of the CdTe layers in a direction perpendicular to the growth plane.

The most intense and narrow rocking curves of CdTe(111) (Figure 4, b) are observed from samples 15 and 18 grown at temperatures of 450 and 400 °C, respectively. The half-width values of these peaks are very close. When the growth temperature decreases to 325 °C (sample 9),

Table 2. Crystal structure features of grown CdTe films

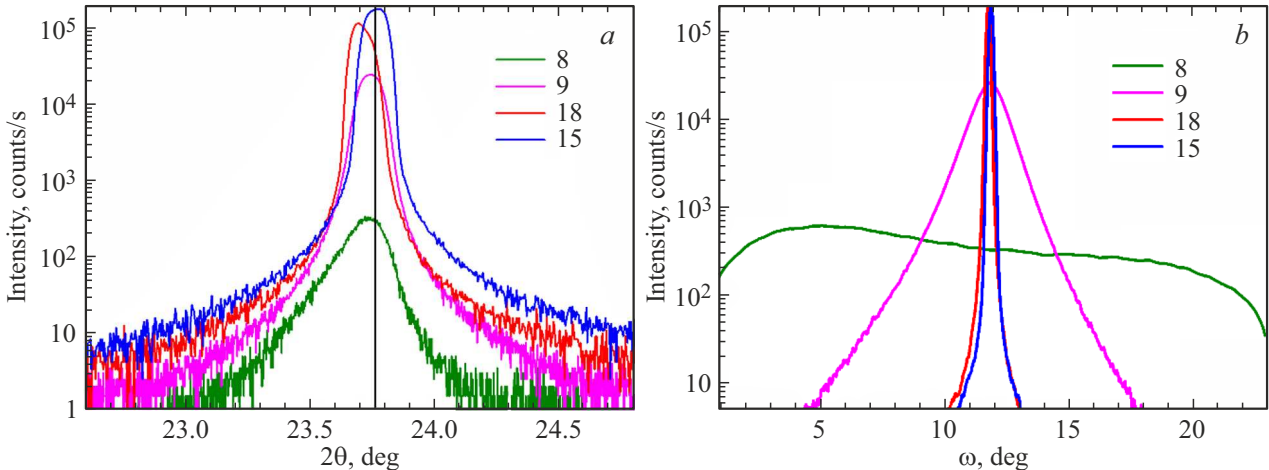


**Figure 4.** RC of CdTe films:  $a - 2\theta/\omega$ -geometry, the vertical line indicates the calculated position of the reflection line CdTe(111),  $b - \omega$ -geometry (rocking curves).

we observe a significant increase in the half-width of the  $\omega$ -peak to 1.48°. Thus, sample 9 contains small-angle blocks of CdTe(111) that are weakly disoriented relative to each other, i.e. it is a mosaic single crystal [22]. The presence of a large number of slightly misoriented blocks in a relatively good single crystal is equivalent to the presence of a large number of dislocations in this crystal, and the boundaries between the blocks are also called small-angle dislocation boundaries [23]. For a sample 8 ( $T_g = 250\,^{\circ}$ C), the rocking curve is a wide plateau with a width of  $\sim 20^{\circ}$ . Therefore, sample 8 is a polycrystal with a distinct grain orientation (textured polycrystal) [22].

The crystal quality of MBE CdTe films was evaluated in Ref. [20] by the width value of FWHM of RC measured in the  $\omega$ -mode (the so-called rocking curve). This parameter characterizes the mutual misorientation of blocks of a mosaic single crystal with the same lattice parameter. The lowest obtained value of FWHM $_{\omega}$  was 280" for 1.7  $\mu$ m thick CdTe(111) film grown at 365 °C, with a nucleus layer thickness of  $\sim$  100 nm, grown at 302 °C. This value is half of our best value of FWHM $_{\omega}$  for film 18 (540"). At the same time, the RMS roughness of the mentioned film from Ref. [20] in terms of area  $5\times5\,\mu$ m was 0.76 nm, which

practically coincides with the roughness of our film 15 (0.71 nm).

To study the orientation of CdTe grains in the substrate plane, the asymmetric reflection of CdTe(422) was analyzed when the sample was rotated 360° around its own axis  $(\varphi$ -scan). To illustrate the measurement scheme, a stereographic projection of reflections from some crystallographic planes of an ideal cubic crystal in polar coordinates with surface orientation (111) is shown in Figure 5, a. The polar radius from 0 to 90° corresponds to the angle of deviation of the corresponding crystallographic directions from the direction (111) located in the center of the circle. The polar angle (from 0 to 360°) corresponds to the angle  $\varphi$  of rotation of the crystal around the normal to the surface, i.e. around the direction (111). The stereographic projection of the crystal with orientation (111) has an axis of symmetry of the 3rd order with respect to rotation around the central axis (111). So, there are 3 reflections from the planes (422) on the stereographic projection deviated by 19.471° from the direction (111). The measuring system was adjusted to an asymmetric Bragg reflection from one of the planes of the family  $\{422\}$  during  $\varphi$ -scanning, after which the sample rotated around the surface normal. For a single crystal

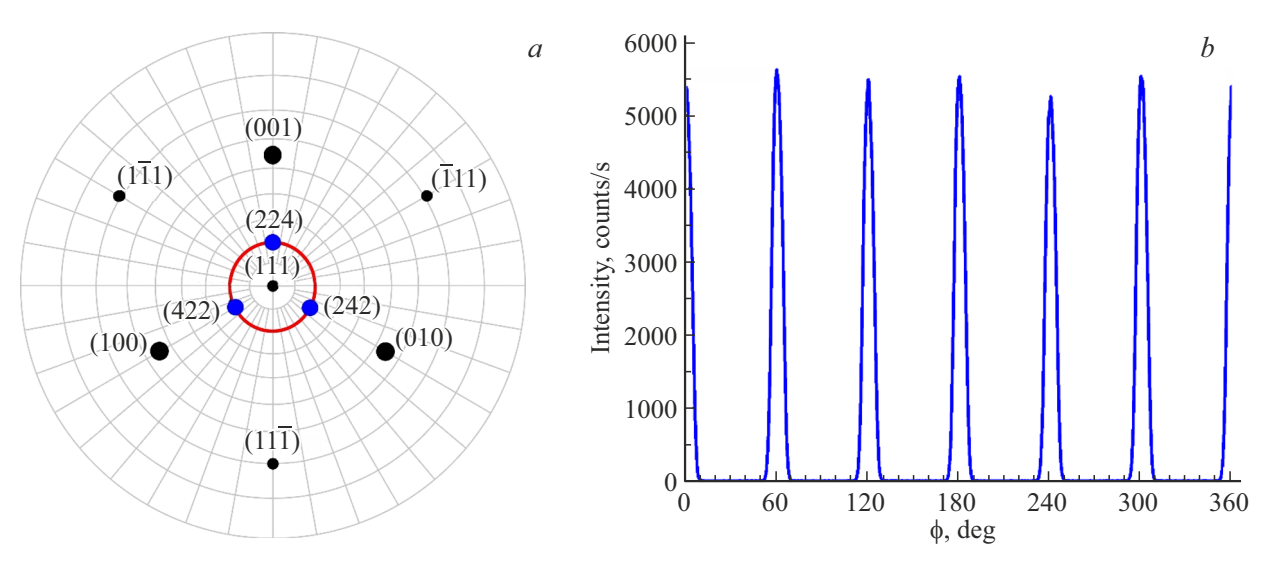


**Figure 5.** Measurement of  $\varphi$ -scans of asymmetric reflection of CdTe(422): a — illustration of a measurement scheme on a stereographic projection of various reflections of a cubic crystal (blue circles show reflections from equivalent planes {422},  $\varphi$ -scan is shown in a red circle), b — $\varphi$ -scan of reflection of CdTe (422) for sample 18.

 $\varphi$ -scan would consist of only three maxima separated by a rotation angle of 120°.

However, there are six maxima of the same intensity on the  $\varphi$ -scan for sample 18 (Figure 5, b), separated by a rotation angle of 60°, in contrast to the expected pattern with three peaks. This pattern is typical for crystals containing twinning defects with crystal domains characterized by a rotation of  $60^{\circ}$  around the axis (111) [24]. The even and odd peaks on the  $\varphi$ -scan correspond to the reflection from one of the two families of twins. The same amplitude of the even and odd peaks indicates the same number and size of the twins of the two orientations. Similar  $\varphi$ -scans were observed for samples 9 and 15. Thus, samples 9, 15, and 18 are single crystals saturated with twinning defects. A weak scattering signal from sample 8 is observed on the  $\varphi$ -scan, independent of the angle of rotation, i.e., there is no predominant orientation of the grains in the substrate plane.

Figure 6 shows the PL spectra of the studied samples. The PL intensity from a sample of 15 is at least an order of magnitude higher than the PL intensity from monocrystalline substrates GaAs(100). A dominant peak with an energy position corresponding to the band gap of CdTe is observed in the PL spectra from samples 15 and 18 at a temperature of 77 K [21].

In addition, some equidistant oscillations are visible on the spectra of samples 15 and 18. Assuming that they are caused by the interference of PL radiation in films with smooth boundaries (the RMS roughness of which does not exceed  $1.5 \, \text{nm}$ ), and also assuming that this radiation propagates from the edge of the film, we estimate the thickness of the films. Let k be an integer number of wavelengths that fit into the path difference of the rays, one of which came out of the CdTe film and the other reflected

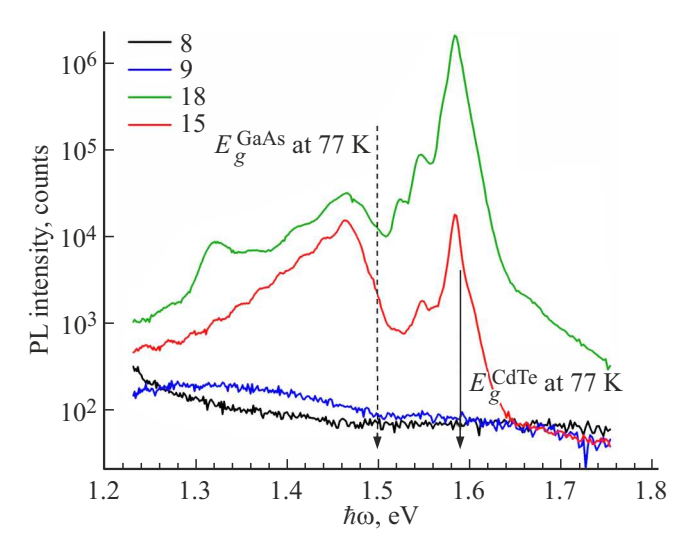


**Figure 6.** PL spectra of the studied samples measured at  $T = 77 \,\mathrm{K}$ .

from the GaAs substrate. Nine oscillations are observed on the PL spectrum of sample 18. To minimize the error, we consider two extreme ones of them: at  $\lambda_1 = 849.1$  nm and  $\lambda_9 = 985.6$  nm. We obtain:  $\lambda_1 \cdot (k+8+1/2) = 2dn_1$ ;  $\lambda_9 \cdot (k+1/2) = 2dn_9$ , where d is the film thickness,  $n_1 = 2.88 - 2.96$  and  $n_9 = 2.77 - 2.85$  is the refractive index CdTe at  $\lambda_1$  and  $\lambda_9$  respectively [25–27]. We find the thickness of the film  $d \approx (6.9 \pm 0.1) \, \mu \text{m}$ . It can be argued that similar oscillations on the PL spectrum of the film 15 are located about half as often as the oscillations on the film 18, hence the conclusion that the film 18 is about twice as thin. Once again, we emphasize that a very primitive model was used to estimate the film thickness, which probably does not fully take into account the mechanism of oscillation

formation on the PL spectra, since in reality the point (or points) of divergence of the two rays is probably not at the film boundary, but at some depth, as a result of which the obtained film thickness has a purely estimated value.

A wide asymmetric peak in the PL spectra of more structurally perfect samples 15 and 18 in the region of 1.40-1.50 eV with a peak at 1.46 eV can be explained by impurity PL, defective PL, or dislocation PL. It is known from the literature [28] that CdTe doping with arsenic with concentration  $2.2 \cdot 10^{18} \, \text{cm}^{-3}$  causes a wide peak at  $T = 4 \,\mathrm{K}$  in the range of  $1.45 - 1.52 \,\mathrm{eV}$  with a peak of 1.49 eV. Energy levels of impurity ions Fe<sup>2+</sup> [29], complexes with Cd [19] vacancies may also appear in the area of interest to us. On the other hand, it has been experimentally shown in Ref. [30] that 60-degree dislocations in CdTe crystals form energy levels in the band gap, which appear on PL spectra at temperatures of 4.2-100 K as a series of peaks (usually three peaks) in the range of 1.47-1.51 eV. However, these peaks were accompanied by a much more intense band near 1.54 eV, which was ultimately associated with 60-degree Cd dislocations, while nothing of the kind was observed in our experiment. Taking into account this consideration, as well as the fact that samples 15 and 19 are not saturated with dislocations (unlike sample 9), we will assign a peak at 1.46 eV to impurity PL.

There is no PL signal from samples 8 and 9, and their PL spectra do not contain pronounced peaks. This indicates the presence of additional energy levels inside the CdTe band gap associated with point defects caused by suboptimal CdTe growing conditions. At the defect levels, nonradiative relaxation of photoexcited electrons occurs, which leads to the disappearance of PL from the CdTe film. By analogy with InGaAs, we can assume that extended defects (dislocations, twins, packing defects) observed by X-ray diffractometry do not cause nonradiative recombination, and its cause is the presence of point defects, to which diffractometry is less sensitive than PL spectroscopy [31].

# 4. Conclusion

The orientation of CdTe films at all growth temperatures is predominantly (111). The crystalline perfection of the film is optimal at a growth temperature of 400-450 °C and deteriorates significantly when the growth temperature drops to 325 °C and below. The most perfect grown films are single crystals containing twinning defects with a very smooth surface. The RMS roughness is minimal and amounts to 0.8 nm at 400 °C. When the growth temperature rises to 450 °C, the surface of the film as a whole becomes slightly more rough, and the surface morphology is more heterogeneous: meander-shaped dips and smooth areas between them are covered with triangular 60-degree steps. However, the intensity of the band-edge PL increases, which may indicate a decrease in the concentration of point defects in the grown film.

A mosaic single crystal with small-angle blocks containing twins is formed at 325 °C, and a textured polycrystal is formed at 250 °C. In all cases where it was possible to clearly observe the orientation of the twins on the  $\varphi$ -scan, the concentration of the two types of twins was the same. Films grown at 325 and 250 °C are saturated with centers of nonradiative recombination (possibly with point defects), leading to complete quenching of the band-edge PL. When the growth temperature rises to 450 °C, a single crystal is also formed, however, in general, its surface is slightly more rough, and the surface morphology is more heterogeneous. In addition, the intensity of the bandedge PL decreases, which may indicate an increase in the concentration of nonradiative recombination centers (possibly — point defects) in the grown film.

Twinning defects present in high-temperature CdTe samples will inevitably pass into the overlying active layers of the HgCdTe. It is possible that these defects will play the role of current leakage lines and centers of nonradiative recombination, however, the latter assumption is opposed by a rather intense band-edge PL from high-temperature samples, comparable to the PL of epitaxial defect-free GaAs.

## **Acknowledgments**

The authors would like to thank the 2nd category engineer of JSC Orion R & P Association A.S. Sukhanova forconducting AFM measurements.

#### Conflict of interest

The authors declare no conflict of interest.

### References

- [1] R. Furstenberg, J.O. White, G.L. Olson. J. Electron. Mater., 34 (6), 791 (2005). https://doi.org/10.1007/s11664-005-0022-8
- [2] M.A. Quijada, A.M. Russell, R.J. Hil. Proc. SPIE 5904, Cryogenic Optical Systems and Instruments XI (18 August 2005), 59040Q. https://doi.org/10.1117/12.618734
- [3] Sh.O. Eminov, A.A. Rajabli, T.I. Ibragimov. Inorg. Mater., **46** (7), 714 (2010). DOI: 10.1134/S0020168510070058
- [4] M. Carmody, A. Yulius, D. Edwall, D. Lee, E. Piquette, R. Jacobs, D. Benson, A. Stoltz, J. Markunas, A. Almeida. J. Electron. Mater., 41, 2719 (2012). https://doi.org/10.1007/s11664-012-2129-z
- [5] V.S. Varavin, S.A. Dvoretsky, D.G. Ikusov, N.N. Mikhailov, V.G. Craftsman, G.Yu. Sidorov, Yu.G. Sidorov, P.V. Sizikov, I.N. Uzhakov. Avtometrija., 49 (5), 68 (2013). (in Russian). https://www.elibrary.ru/item.asp?id=20501810
- [6] W. Lei, R.J. Gu, J. Antoszewski, J. Dell, G. Neusser, M. Sieger, B. Mizaikof, L. Faraone. J. Electron. Mater., 44, 3180 (2015). https://doi.org/10.1007/s11664-015-3876-4
- [7] W. Lei, Y.L. Ren, I. Madni, L. Faraone. Infr. Phys. Technol., 92, 96 (2018). https://doi.org/10.1016/j.infrared.2018.05.010

- [8] M.F. Vilela, K.R. Olsson, E.M. Norton, J.M. Peterson, K. Rybnicek, D.R. Rhiger, C.W. Fulk, J.W. Bangs, D.D. Lofgreen, S.M. Johnson. J. Electron. Mater., 42, 3231 (2013). https://doi.org/10.1007/s11664-013-2798-2
- [9] V.S. Varavin, V.V. Vasiliev, A.A. Guzev, S.A. Dvoretsky, A.P. Kovchavtsev, D.V. Marin, I.V. Sabinina, Yu.G. Sidorov, G.Yu. Sidorov, A.V. Tsarenko, M.V. Yakushev. FTP, 50 (12), 1652 (2016). (in Russian). DOI: 10.21883/ftp.2016.12.43894.40
- [10] M.F. Vilela, D.D. Lofgreen, E.P.G. Smith, M.D. Newton, G.M. Venzor, J.M. Peterson, J.J. Franklin, M. Reddy, Y. Thai, E.A. Patten, S.M. Johnson, M.Z. Tidrow. J. Electron. Mater., 37, 1465 (2008). https://doi.org/10.1007/s11664-008-0443-2
- [11] M.V. Yakushev, D.V. Brunev, V.S. Varavin, V.V. Vasiliev, S.A. Dvoretskii, I.V. Marchishin, A.V. Predein, I.V. Sabinina, Yu.G. Sidorov, A.V. Sorochkin. FTP, 45 (3), 396 (2011). (in Russian).https://journals.ioffe.ru/articles/viewPDF/7374
- [12] I.V. Sabinina, A.K. Gutakovsky, Yu.G. Sidorov, A.V. Latyshev.
  J. Cryst. Growth, 274, 339 (2005).
  https://doi.org/10.1016/j.jcrysgro.2004.10.053
- [13] M. Reddy, J.M. Peterson, T. Vang, J.A. Franklin, M.F. Vilela, K. Olsson, E.A. Patten, W.A. Radford, J.W. Bangs, L. Melkonian, E.P.G. Smith, D.D. Lofgreen, S.M. Johnson. J. Electron. Mater., 40 (8), 1706 (2011). DOI: 10.1007/s11664-011-1665-2
- [14] W. Lei, J. Antoszewski, L. Faraone. Appl. Phys. Rev., 2, 041303 (2015). DOI: 10.1063/1.4936577
- [15] V.S. Varavin, S.A. Dvoretsky, N.N. Mikhailov, V.G. Craftsman, I.V. Sabinina, Yu.G. Sidorov, V.A. Shvets, M.V. Yakushev, A.V. Latyshev. Avtometriya, 56 (5), 12 (2020). (in Russian). DOI: 10.15372/AUT20200502
- [16] K.H. Lee, J.H. Jung, T.W. Kim, H.S. Lee, H.L. Park. Appl. Surf. Sci., 253 (20), 8470 (2007). DOI: 10.1016/j.apsusc.2007.04.019
- [17] Y.G. Sidorov, M.V. Yakushev, A.V. Kolesnikov. Avtometrija, 50 (3), 25 (2014). https://www.sibran.ru/journals/issue.php?ID=161181
- [18] M.S. Kwon, J.Y. Lee, M.D. Kim, T.W. Kang. J. Cryst. Growth, **186** (1), 79 (1998). DOI: 10.1016/S0022-0248(97)00442-9
- [19] K. Koike, T. Tanaka, S. Li, M. Yano. J. Cryst. Growth, 227-228, 671 (2001). https://doi.org/10.1016/S0022-0248(01)00800-4
- [20] S.X. Zhang, J. Zhang, X.F. Qiu, Y. Wu, P.P. Chen. J. Cryst. Growth, 546, 125756 (2020).
  DOI: 10.1016/j.jcrysgro.2020.125756
- [21] S. Adachi. *Properties of Semiconductor Alloys: Group-IV, III–V and II–VI Semiconductors* (John Wiley & Sons, Ltd, 2009). ISBN: 978-0-470-74369-0
- [22] S.F. Solodovnikov. *Osnovnye terminy i ponyatiya strukturnoj kristallografii i kristallokhimii* (slovar-posobie) (Novosibirsk, INH SO RAN, 2005) p. 51. (in Russian).
- [23] Van Buren. Defekty v kristallakh, per. s angl. pod red. A.N.Orlov and V.R.Regel. (M., Izd-vo inostr. lit., 1962). (in Russsian).
- [24] A. Klochkov, A. Vinichenko, A. Samolyga, S. Ryndya, M. Poliakov, N. Kargin, I. Vasil'evskii. Appl. Surf. Sci., 619, 156722 (2023). DOI: 10.1016/j.apsusc.2023.156722
- [25] R.E. Treharne, A. Seymour-Pierce, K. Durose, K. Hutchings,
  S. Roncallo, D. Lane. J. Phys.: Conf. Ser., 286, 012038 (2011).
  DOI: 10.1088/1742-6596/286/1/012038
- [26] M.N. Polyanskiy. Sci. Data, 11, 94 (2024).DOI: 10.1038/s41597-023-02898-2

- [27] S. Adachi, T. Kimura, N. Suzuki. J. Appl. Phys., 74, 3435 (1993). http://dx.doi.org/10.1063/1.354543
- [28] V.S. Evstigneev, A.V. Chilyasov, A.N. Moiseev, S.V. Morozov,
  D.I. Kuritsyn. FTP, 55 (1), 9 (2021). (in Russian).
  DOI: 10.21883/FTP.2021.01.50377.9514
- [29] I.S. Kurchatov, E.F. Kustov. FTP, 52 (7), 679 (2018). (in Russian).
  DOI: 10.21883/FTP.2018.07.46034.8542
- [30] N.I. Tarbaev, G.A. Shepelsky. FTP, 40 (10), 1175 (2006). (in Russian). https://journals.ioffe.ru/articles/viewPDF/6163
- [31] I.S. Vasilevsky, S.S. Pushkarev, M.M. Grekhov, A.N. Vinichenko, D.V. Lavrukhin, O.S. Kolentsova. FTP, 50 (4), 567 (2016). (in Russian). https://journals.ioffe.ru/articles/viewPDF/43006

Translated by A.Akhtyamov